

Sequential Monte Carlo Squared for Online Inference in Stochastic Epidemic Models

Dhorasso Temfack and Jason Wyse

School of Computer Science and Statistics, Trinity College Dublin, Ireland

Abstract

Effective epidemic modeling and surveillance require computationally efficient methods that can continuously update parameter estimates as new data becomes available. This paper explores the application of an online variant of Sequential Monte Carlo Squared (O-SMC²) to the stochastic Susceptible-Exposed-Infectious-Removed (SEIR) model for real-time epidemic tracking. The advantage of O-SMC² lies in its ability to update parameter estimates using a particle Metropolis-Hastings kernel by only utilizing a fixed window of recent observations. This feature enables timely parameter updates and significantly enhances computational efficiency compared to standard SMC², which by comparison, requires processing of all past observations. First, we demonstrate the efficiency of O-SMC² on simulated epidemic data, where both the true parameter values and the observation process are known. We then make an application to a real-world COVID-19 dataset from Ireland, successfully tracking the epidemic and estimating a time-dependent reproduction number of the disease. Our results show that O-SMC² provides highly accurate online estimates of both static and dynamic epidemiological parameters while substantially reducing computational cost. These findings highlight the potential of O-SMC² for real-time epidemic monitoring and supporting adaptive public health interventions.

Keywords: Disease modeling, Stochastic model, Sequential Monte Carlo, Online inference

1 Introduction

Disease modeling plays a crucial role in public health by providing insights into the mechanisms behind the spread of infectious diseases. Such understanding is vital for designing effective intervention strategies and supporting evidence-based policy-making. As the global landscape of infectious diseases evolves and the risk of novel a pandemic events like COVID-19 increases (Marani et al., 2021), there is a pressing need for robust modeling frameworks that can adapt to changes in the underlying disease dynamics, progressively update parameter values as new information becomes available, and deliver accurate assessments and predictions of epidemic trajectories (Birrell et al., 2017).

Traditionally, parameter inference in epidemic models has been approached using both frequentist and Bayesian methods. Frequentist techniques such as maximum likelihood estimation (Althaus, 2014) and nonlinear least squares (Aloke et al., 2023) have been widely applied to deterministic models based on ordinary differential equations due to their simplicity and computational efficiency. Bayesian approaches, have gained popularity for their ability to incorporate prior knowledge and quantify uncertainty. In this context, Markov chain Monte Carlo (MCMC) methods remain a popular choice for sampling from posterior distributions of model parameters (O'Neill and Roberts, 1999; Jewell et al., 2009; Wang and Walker, 2022). Recent advances in probabilistic programming tools like Stan (Carpenter et al., 2017; Grinsztajn et al., 2021) and specialized toolboxes such as `quantdiffforecast` (Chowell et al., 2024) and `Bayesianfitforecast` (Karami et al., 2024) have made Bayesian workflows more accessible and flexible in epidemiological modeling. However, the computational demands of MCMC limit its utility for real-time applications. This is because incorporating incrementally observed new data points typically necessitates re-running the

entire inference process (Birrell et al., 2017). When the likelihood function is intractable but simulation from the generative model is feasible, likelihood-free approaches such as Approximate Bayesian Computation (ABC) are commonly used (Kypriaios et al., 2017). While ABC methods offer flexibility and an intuitive framework, their performance relies heavily on a user chosen set of summary statistics to measure the distance between simulated and observed data. Poorly chosen, these can detrimentally impact performance. Standard ABC lacks native mechanisms for sequential parameter updating as new data arrive incrementally (Minter and Retkute, 2019). Sequential adaptations of ABC are possible (Toni et al., 2009), however these still depend heavily on user chosen summary statistics, creating challenges in complex modelling scenarios (Han et al., 2025).

We adopt an approach which gets around many of the limitations outlined above, and enables sequential and probabilistically well calibrated inference. Sequential Monte Carlo (SMC) methods, also known as particle filtering, provide a natural framework for real-time state and parameter estimation by sequentially updating a posterior distribution as new data becomes available (Doucet et al., 2001). These methods have seen growing application in epidemiology, with early studies demonstrating their effectiveness in calibrating nonlinear compartmental models of infectious disease dynamics (Yang et al., 2014; Cama-cho et al., 2015). For example, Welding and Neal (2019) applied a sequential Bayesian framework to the 2001 UK Foot-and-Mouth epidemic, using MCMC-based rejuvenation steps to mitigate particle degeneracy and enable real-time outbreak analysis. Similarly, Birrell et al. (2020) developed an age-structured SEIR model on simulated influenza outbreak data, demonstrating efficient real-time inference by integrating multiple data sources and reducing computational costs compared to standard MCMC.

While SMC methods are well-suited for sequential state estimation, they are not directly able to facilitate the estimation of static parameters (Kantas et al., 2015). Hybrid techniques such as particle MCMC (PMCMC) (Andrieu et al., 2010) address this limitation by combining SMC with MCMC. PMCMC generates unbiased likelihood estimates through particle filtering, enabling exact posterior sampling via traditional MCMC methods. However, these methods remain computationally demanding since each MCMC iteration requires a full SMC run, limiting their suitability for real-time applications (Dureau et al., 2013; Funk et al., 2018; Endo et al., 2019; Cazelles et al., 2021). In their recent study, Storvik et al. (2023) propose an SMC framework for inferring a time-varying reproduction number of COVID-19 in Norway. Their approach sequentially estimates hyperparameters controlling the reproduction number by relying on a set of sufficient statistics. However, this approach assumes that the sufficient statistics-based filters are analytically tractable, a condition that only holds for particular types of dynamical systems.

A promising alternative is the SMC² algorithm (Chopin et al., 2013; Jacob, 2015; Rosato et al., 2023), which integrates nested particle filters to simultaneously estimate model states and parameters, improving both accuracy and adaptability. A key step in SMC² is the so-called “rejuvenation” using PMCMC kernels to prevent particle impoverishment. Nevertheless, this step conventionally requires computing the likelihood over all past observations, posing challenges for truly online or streaming data applications.

To address this limitation, Vieira (2018) introduced a computationally efficient modification that evaluates the PMCMC over a fixed-size moving window of recent observations. In this study, we apply and evaluate this fixed-window SMC² approach, referred to as online SMC² (O-SMC²), within the context of epidemic modeling. While O-SMC² is an established algorithm, its strengths for disease modeling have not been explored. Our contribution is its tailored implementation and comprehensive assessment for sequential state and parameter inference in stochastic SEIR models under real-time constraints. This is an area of growing practical importance for epidemic response planning. Compared to standard SMC², the O-SMC² framework substantially reduces computational demands while preserving the capacity for accurate sequential estimation. This efficiency gain is particularly relevant for fast-moving outbreaks, where timely estimates of key epidemiological

parameters such as the time-varying effective reproduction number and the infectious period are critical for guiding public health interventions.

The remainder of this paper is structured as follows. Section 2 describes the state-space framework for the SEIR compartmental model, provides a brief overview of the SMC²/O-SMC² methodology, and discusses parameter identifiability. In Section 3, we apply the O-SMC² algorithm to both simulated data and real-world COVID-19 data from Ireland, demonstrating its potential for real-time epidemiological surveillance and inference of the time-dependent reproduction number. Finally, Section 4 concludes the paper by summarizing the main findings and discussing potential challenges and limitations of our approach.

2 Compartmental model and sequential inference

2.1 Stochastic SEIR model

Compartmental models for infectious diseases, which had their conceptual origins in the early to mid 20th century, attempt to describe a disease’s progression and spread through individuals moving through disease stages over time. The stochastic SEIR model serves as the foundation for our investigation. Consider the time interval $(t, t + \delta t]$, where δt represents the time between observations. If we assume that the time spent by an individual in a compartment is exponentially distributed with a rate λ , then the number of individuals leaving a compartment during the time step δt can be seen as a Binomial random variable with success probability $p = 1 - e^{-\lambda\delta t}$ (this parameterization ensures a success probability between 0 and 1, see [Lekone and Finkenstädt \(2006\)](#)). The discrete-time SEIR stochastic model is specified by:

$$\begin{aligned} S_{t+\delta t} &= S_t - Y_{SE}(t), & Y_{SE}(t) &\sim \text{Bin}\left(S_t, 1 - e^{-\beta \frac{I_t}{N} \delta t}\right) \\ E_{t+\delta t} &= E_t + Y_{SE}(t) - Y_{EI}(t), & Y_{EI}(t) &\sim \text{Bin}\left(E_t, 1 - e^{-\sigma \delta t}\right) \\ I_{t+\delta t} &= I_t + Y_{EI}(t) - Y_{IR}(t), & Y_{IR}(t) &\sim \text{Bin}\left(I_t, 1 - e^{-\gamma \delta t}\right) \\ R_{t+\delta t} &= R_t + Y_{IR}(t). \end{aligned} \quad (1)$$

Here, S_t , E_t , I_t , and R_t represent the compartments of susceptible, exposed (infected but not yet infectious), infectious, and removed individuals, respectively, at time t . Susceptible individuals, upon contact with infectious individuals, transition to the exposed class at a rate β (which can be time-dependent or constant). Exposed individuals become infectious at a rate σ , and infectious individuals recover from the disease at a rate γ (Figure 1). The population is assumed to have a constant size $N = S_t + E_t + I_t + R_t$ at each time point.

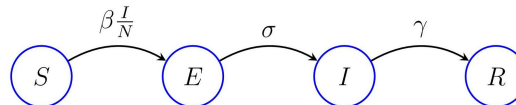


Fig. 1: Graphical representation of a SEIR model. Each arrow expresses the rate of transition between the compartments. β is the disease transmission rate, $1/\sigma$ is the mean incubation period, and $1/\gamma$ is the mean infectious period.

2.2 State-space framework

In the context of the SEIR model, the system can be formulated as a state-space model (SSM), which consists of two stochastic processes: one governing the evolution of the disease within the population, and the other describing the observation process (Figure 2).

The state-space model is defined for time steps $t = 1, \dots, T$ as follows:

$$x_0 \sim f(x_0|\theta), \quad \triangleright \quad \text{Initial state} \quad (2)$$

$$x_t|x_{t-1} \sim f(x_t|x_{t-1}, \theta), \quad \triangleright \quad \text{State transition process} \quad (3)$$

$$y_t|x_t \sim g(y_t|x_t, \theta). \quad \triangleright \quad \text{Observation process} \quad (4)$$

Here, x_t denotes the vector of latent state variables (state variable in the classical SEIR model), which evolve according to a Markov process with transition distribution $f(x_t|x_{t-1}, \theta)$ given by the model (1). The observation y_t is assumed to be probabilistically related to the hidden state x_t via the distribution $g(y_t|x_t, \theta)$. The parameter vector θ encompasses all static epidemiological parameters of the model such as β , σ and γ , governing both the state transitions and the observation process. Throughout the study, θ refers collectively to all state space model and observation process parameters.

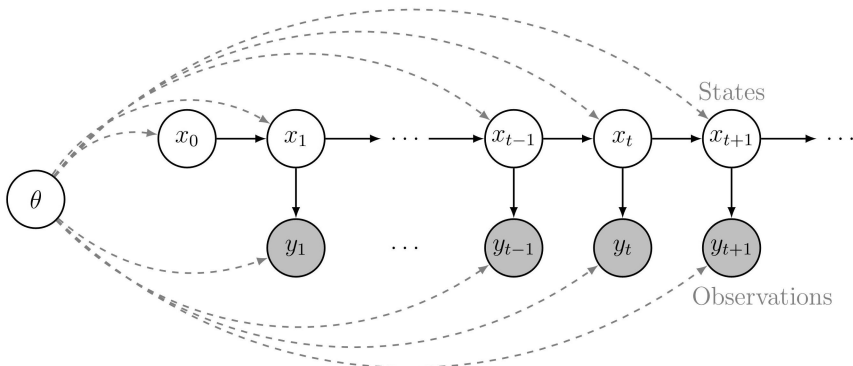


Fig. 2: Graphical representation of a state-space model. Black arrows show variable dependencies, and dashed gray lines represent the dependence on θ .

State-space models are particularly useful for modeling complex dynamical systems such as disease transmission where the true states are not directly observable, and observations are subject to noise or other forms of uncertainty. By explicitly modeling the hidden states and their relationship to observed data, we can perform inference on both the state variables and the model parameters.

2.3 State and Parameter inference

In this section, we briefly describe the procedure for sequential parameter estimation using the SMC² scheme. Let $x_{0:t}$ ¹ represent the sequence of latent states (in our case the SEIR compartment counts) up to time t , and let $y_{1:t}$ represent the observations (e.g., daily reported cases). The goal is to construct a sequence of posterior distributions $\{p(\theta|y_{1:t}), t = 1, \dots, T\}$ that reflect the evolution of parameter estimates as new observations become available. Bayes' rule provides the basis for updating the posterior distribution as follows:

$$p(\theta|y_{1:t}) \propto p(\theta|y_{1:t-1})p(y_t|y_{1:t-1}, \theta), \quad (5)$$

which suggests a sequential importance sampling approach. This approach involves reweighting a set of parameter particles based on the incremental likelihood $p(y_t|y_{1:t-1}, \theta)$. The iterated batch importance sampling (IBIS) method (Chopin, 2002) employs this technique with an MCMC step to rejuvenate parameter samples. However, for state-space models, the incremental likelihood is generally intractable. To address this issue, we can replace $p(y_t|y_{1:t-1}, \theta)$ with an unbiased estimate derived from running a particle filter, targeting the filtering distribution $p(x_t|y_{1:t}, \theta)$ for each of the θ -particles. This approach is known as SMC² due to the use of nested filters. For a comprehensive discussion on this approach, including formal justifications, refer to (Chopin et al., 2013).

¹ For any sequence $\{y_t\}_{t \geq 0}$, we denote $z_{i:j} = \{z_i, z_{i+1}, \dots, z_j\}$ and $z_j^{1:N}$ (resp. $z_{i:j}^{1:N}$) is a set of N random variables z_j^l (resp. $z_{i:j}^l$), for $l = 1, \dots, N$.

2.3.1 Particle filtering

For a given value of the model parameters θ , the latent variables x_t at each time point, can be inferred from the observations $y_{1:t}$ using the filtering distribution $p(x_t|y_{1:t}, \theta)$. Particle filtering is a technique that approximates this filtering distribution by sequentially generating a set of particles with associated weights $\{x_t^i, w_t^i\}_{i=1}^{N_x}$, via importance sampling and resampling. Hence, for a known parameter value θ , the posterior distribution of the latent states is represented as a Dirac delta mixture:

$$p(x_t|y_{1:t}, \theta) \approx \frac{1}{\sum_{j=1}^{N_x} w_t^j} \sum_{i=1}^{N_x} w_t^i \delta_{x_t^i}(x_t). \quad (6)$$

Here, N_x denotes the number of x -particles, and $w_t^i := w_t^i(x_{t-1}^i, x_t^i)$ represents the importance weight for each particle x_t^i . The weight update rule at time t takes into account both the likelihood of the new observation y_t given the current particle state x_t^i , and the transition probability between successive states:

$$w_t^i = w_{t-1}^i \frac{g(y_t|x_t^i, \theta) f(x_t^i|x_{t-1}^i, \theta)}{q(x_t^i|x_{t-1}^i, y_t, \theta)}, \quad i = 1, \dots, N_x, \quad (7)$$

One notable particle filtering method is the Bootstrap particle filter (BPF) (Gordon et al., 1993), which simplifies weight calculations by setting the importance distribution equal to the state transition distribution, i.e. $q(x_t|x_{t-1}, y_t, \theta) = f(x_t|x_{t-1}, \theta)$. Many filtering algorithms have been developed to improve efficiency (Pitt and Shephard, 1999), but for this study, we focus on the BPF. The general procedure for the Bootstrap Particle Filter is shown in Algorithm 1.

Algorithm 1 Bootstrap Particle Filter (BPF) for a given parameter θ

Operations involving index i must be performed for $i = 1, \dots, N_x$.

The indices $a_t^{1:N_x}$ define the ancestral particles at time t after the resampling.

Inputs: Observation: $y_{1:T}$, Number of particles: N_x , Initial state distribution: $f(x_0|\theta)$, Parameter vector: θ .

Output: Particle set : $\{x_{0:t}^i, w_{0:t}^i\}_{i=1}^{N_x}$

- 1: Sample initial particles : $x_0^i \sim f(x_0|\theta)$
- 2: Compute weights: $w_0^i = 1, \quad W_0^i = w_0^i / \sum_{j=1}^{N_x} w_0^j$
- 3: **for** $t = 1$ to T **do**
- 4: Sample new indices: $a_t^{1:N_x} \sim \text{Resample}(W_{t-1}^{1:N_x})$
- 5: Propagate states $x_t^i \sim f(x_{t-1}^{a_t^i}, \theta)$
- 6: Compute new weights $w_t^i = g(y_t|x_t^i, \theta), \quad W_t^i = w_t^i / \sum_{j=1}^{N_x} w_t^j$
- 7: **end for**

The resampling step in Algorithm 1, referred to in step 4, aims to mitigate particle degeneracy² by discarding particles with lower weights and duplicating those with higher weights. After resampling, we reset all weights to $w_{t-1}^i = 1$. Various resampling schemes exist as described in Doucet et al. (2009). Unless stated otherwise, we use stratified resampling in all our implementations due to its efficiency and lower computational cost (Sheinson et al., 2014; Vieira, 2018). In Algorithm 1, if the resampling step is omitted, then the weights are replaced by $w_t^i = w_{t-1}^i g(y_t|x_t^i, \theta)$. Particle filtering can also be used for Bayesian parameter inference since it provides an unbiased estimate of the incremental

² Particle degeneracy refers to the situation where, after many iterations, only a small number of particles dominate and retain a large proportion of the weight.

likelihood:

$$p(y_t|y_{1:t-1}, \theta) \approx \hat{p}_{N_x}(y_t|y_{1:t-1}, \theta) = \frac{1}{N_x} \sum_{i=1}^{N_x} w_t^i \quad (8)$$

Using the law of total probability, an SMC estimate of the marginal likelihood at θ follows:

$$p(y_{1:t}|\theta) \approx \hat{p}_{N_x}(y_{1:t}|\theta) = \prod_{s=1}^t \hat{p}_{N_x}(y_s|y_{1:s-1}, \theta) = \prod_{s=1}^t \left(\frac{1}{N_x} \sum_{i=1}^{N_x} w_s^i \right). \quad (9)$$

2.3.2 SMC² scheme

Given a weighted sample $\{\theta_t^m, \omega_t^m\}_{m=1}^{N_\theta}$ from $p(\theta|y_{1:t})$, the SMC² algorithm reweights each θ -particle using an unbiased estimate of the incremental likelihood $p(y_t|y_{1:t-1}, \theta_t^m)$, obtained from the Bootstrap particle filter. Alternative estimates from other filters, such as the auxiliary particle filter, can also be employed to improve efficiency (Golightly and Kypraios, 2018). As we accrue observations through time, there is a risk that only a small number of θ -particles will hold a significant proportion of the weight. To address this, a resampling step is performed to generate a new set of particles from the dominant ones, followed by a PMCMC move step, such as the particle Marginal Metropolis-Hastings (PMMH) kernel, which preserves the target posterior distribution (Andrieu et al., 2010). The combination of the resampling and move steps is referred to as the “rejuvenation” step. In this study, new parameters are proposed from a normal distribution $\theta^* \sim q(\theta^*|\theta_t^m) := \mathcal{N}(\hat{\mu}_t, c\hat{\Sigma}_t)$, where c is a scaling factor. The mean and variance-covariance matrix are given by:

$$\hat{\mu}_t = \frac{1}{\sum_{m=1}^{N_\theta} \omega_t^m} \sum_{m=1}^{N_\theta} \omega_t^m \theta_t^m, \text{ and } \hat{\Sigma}_t = \frac{1}{\sum_{m=1}^{N_\theta} \omega_t^m} \sum_{m=1}^{N_\theta} \omega_t^m (\theta_t^m - \hat{\mu}_t)(\theta_t^m - \hat{\mu}_t)^\top, \quad (10)$$

This allows us to draw new parameter particles in the region where most of the probability mass is located (Chopin, 2002).

The SMC² scheme is outlined in Algorithm 2, and the model evidence can be estimated using the following expression:

$$\hat{Z}_t = \prod_{s=1}^t \left(\frac{1}{\sum_{m=1}^{N_\theta} \omega_{s-1}^m} \sum_{m=1}^{N_\theta} \omega_{s-1}^m \hat{p}_{N_x}(y_s|y_{1:s-1}, \theta_s^m) \right), \quad (11)$$

where $\hat{p}_{N_x}(y_s|y_{1:s-1}, \theta_s^m)$ is the likelihood computed using the particle filter, as described in equation (8). Each rejuvenation (step 8–12 of the Algorithm 2) performs M successive PMMH moves on each particle θ_t^m . The resampling step is similar to the one used in Algorithm 1 but is performed only when a degeneracy criterion is met.

A common way is to estimate the degree of degeneracy by computing the effective sample size (ESS) :

$$\text{ESS}_\theta = \left(\sum_{m=1}^{N_\theta} \omega_t^m \right)^2 / \sum_{m=1}^{N_\theta} (\omega_t^m)^2. \quad (12)$$

The rejuvenation step is triggered if the ESS_θ falls below a specified threshold, typically if $\text{ESS}_\theta < \tau_R N_\theta$, where $\tau_R \in (0, 1)$ is a user-defined parameter. The choice of τ_R controls the frequency of rejuvenation steps: a higher threshold leads to more frequent rejuvenation, increasing computational cost, while a lower threshold reduces the frequency, potentially allowing particle degeneracy to persist. In practice, an ESS threshold of 50% ($\tau_R = 0.5$) is commonly used (Chopin et al., 2013; Jacob, 2015).

Algorithm 2 SMC²

Operations involving index m must be performed for $m = 1, \dots, N_\theta$.

The indices $a_{1:N_\theta}$ define the ancestral particles after the resampling.

Inputs: Observation: $y_{1:T}$, Prior: $p(\theta)$, Number of state particles: N_x , Number of parameter particles: N_θ , Resample threshold : τ_R , Move step: M

Output: Particle set: $\left\{ \theta_{0:t}^m, \omega_{0:t}^m, x_{0:t,\theta_t^m}^{1:N_x}, w_{0:t,\theta_t^m}^{1:N_x} \right\}_{m=1}^{N_\theta}$.

```

1: Sample a initial particles  $\theta_0^m \sim p(\theta)$  and set  $\omega_0^m = 1/N_\theta$ .
2: for  $t = 1$  to  $T$  do
3:   Perform iteration  $t$  of the BPF to obtain  $\left\{ x_{t,\theta_t^m}^{1:N_x}, w_{t,\theta_t^m}^{1:N_x} \right\}$  and  $\hat{p}_{N_x}(y_t|y_{1:t-1}, \theta_t^m)$ .
4:   Update importance weights:  $\omega_t^m = \omega_{t-1}^m \hat{p}_{N_x}(y_t|y_{1:t-1}, \theta_t^m)$ ,  $\omega_t^m = \omega_t^m / \sum_{j=1}^{N_\theta} \omega_t^j$ 
5:   if  $\text{ESS}_\theta < \tau_R N_\theta$  then
6:     Sample new indices  $a_{1:N_\theta} \sim \text{Resample}(\omega_t^{1:N_\theta})$ 
7:     Set  $\{\theta_t^m, \omega_t^m\} := \{\theta_t^{a_m}, 1/N_\theta\}$ ,  $\left\{ x_{t,\theta_t^m}^{1:N_x}, w_{t,\theta_t^m}^{1:N_x} \right\} := \left\{ x_{t,\theta_t^{a_m}}^{1:N_x}, w_{t,\theta_t^{a_m}}^{1:N_x} \right\}$ 
8:     Propose  $\theta^* \sim q(\theta^*|\theta_t^m)$  and perform BPF with  $N_x$  particles given  $\theta^*$  to obtain
    $\hat{p}_{N_x}(y_{1:t}|\theta^*)$ 
9:
10:    Compute :  $\alpha = \min \left\{ 1, \frac{\hat{p}_{N_x}(y_{1:t}|\theta^*)p(\theta^*)}{\hat{p}_{N_x}(y_{1:t}|\theta_t^m)p(\theta_t^m)} \times \frac{q(\theta_t^m|\theta^*)}{q(\theta^*|\theta_t^m)} \right\}$ 
11:
12:    Set  $(\theta_t^m, x_{t,\theta_t^m}^{1:N_x}, w_{t,\theta_t^m}^{1:N_x}) = \begin{cases} (\theta^*, x_{t,\theta^*}^{1:N_x}, w_{t,\theta^*}^{1:N_x}) & \text{with probability } \alpha \\ (\theta_t^m, x_{t,\theta_t^m}^{1:N_x}, w_{t,\theta_t^m}^{1:N_x}) & \text{with probability } 1 - \alpha \end{cases}$ 
13:   end if
14: end for

```

2.4 Online SMC²

While SMC² enables sequential estimation of parameters as new observations arrive, it is not a truly online method. The PMMH step, which has a computational complexity of $\mathcal{O}(tN_\theta N_x)$, requires calculating the marginal likelihood $p(y_{1:t}|\theta)$. Consequently, the computational cost increases with the number of observations t , making the method increasingly expensive as more data accumulates. Although [Chopin et al. \(2013\)](#) demonstrates that, in theory, the frequency at which the rejuvenation step is performed will decrease over time, the algorithm may still be impractical for some real-time applications. [Vieira \(2018\)](#) proposes to implement SMC² in an online manner (O-SMC²) by calculating the likelihood using only a fixed-size window of past observations. This restriction keeps the computational cost of a likelihood calculation constant. By considering a fixed window of observations of size $t_k > 0$ in the PMMH, we can ensure that the online part of SMC² will not be altered, and the online approximation will target the posterior of the parameters given the observation window $p(\theta|y_{t-t_k+1:t})$. This reduces the computational cost of each PMMH iteration from $\mathcal{O}(tN_\theta N_x)$ to $\mathcal{O}(t_k N_\theta N_x)$.

Hence, in step 8 of Algorithm 2, once we have reached $t > t_k$, the Metropolis-Hastings acceptance probability will now take the form:

$$\min \left\{ 1, \frac{\hat{p}_{N_x}(y_{t-t_k+1:t}|\theta^*)p(\theta^*)}{\hat{p}_{N_x}(y_{t-t_k+1:t}|\theta_t^m)p(\theta_t^m)} \times \frac{q(\theta_t^m|\theta^*)}{q(\theta^*|\theta_t^m)} \right\}, \quad (13)$$

where the estimate of the marginal likelihood within the time window is computed similarly to (9), but this time using the restricted particle set $x_{t-t_k+1:t}^{1:N_x}$ (see B for further details) :

$$\hat{p}_{N_x}(y_{t-t_k+1:t}|\theta) = \prod_{s=t-t_k+1}^t \left(\frac{1}{N_x} \sum_{i=1}^{N_x} w_s^i(x_{s-1}^i, x_s^i) \right). \quad (14)$$

This restriction is possible under the assumption that static parameters will remain constant indefinitely (Vieira, 2018). The O-SMC² scheme appears to be particularly amenable to parallelization over parameter particles, as the rejuvenation step can be performed separately for each parameter value.

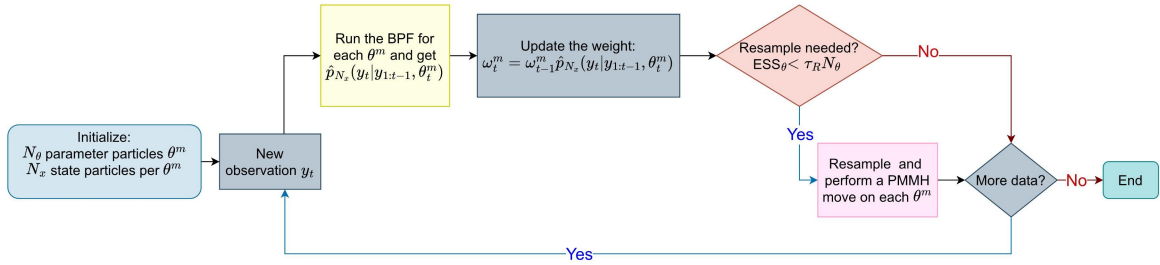


Fig. 3: Flowchart of the SMC²/O-SMC² algorithm.

Figure 3 illustrates the flow of the SMC²/O-SMC² algorithm. At each time step, a new observation y_t arrives. A particle filter is run for each parameter particle θ^m to estimate the likelihood and update the weights. If resampling is needed, it is followed by a PMMH rejuvenation step. The procedure repeats as new observations arrive, allowing for sequential joint inference of parameters and latent states.

2.5 Structural identifiability

Prior to presenting the inference results using the O-SMC² methodology in Section 3, we conduct a structural identifiability analysis of the SEIR model parameters. This analysis employed a deterministic mean-field approximation (Roberts et al., 2015) of the stochastic model given in Equation (1) and was performed using the `StructuralIdentifiability.jl` package in Julia (Dong et al., 2023; Liyanage et al., 2025). The results indicate that the parameters β , σ , and γ are globally identifiable from ideal observations of the daily incidence. This provides a theoretical basis supporting the feasibility of parameter estimation under perfect data conditions. Further details of the model formulation and the output function used are provided in Appendix A.

However, it is important to emphasize some limitations inherent in structural identifiability analysis. The analysis makes the assumptions of noise-free, continuously reported and complete observations. These assumptions will rarely hold in practical epidemiological settings. Epidemiological data are often sparse, noisy, and collected at discrete time points (for example, daily or weekly reports), and may have missing information. These challenges are especially pronounced in the early stages of an outbreak.

In the context of sequential parameter estimation, when only a small number of observations have been accrued at the early stages of an outbreak, we expect to see high uncertainty, wide credible intervals, and possible parameter confounding (Sauer et al., 2021). Thankfully, this is usually observed only during early phases. With the incorporation of informative priors, these challenges are somewhat mitigated and due to the adaptive qualities of sequential inference, they gradually resolve as we accrue more data. We may also experience challenges during periods of abrupt change in disease dynamics. Parameters may become highly correlated and hence poorly identified. This again can be mitigated through the use of informative priors.

In summary, the conclusions drawn from an identifiability analysis are subject to often unrealisable assumptions in practical settings. In our context, idealized structural analyses should be viewed as necessary but not sufficient conditions for practical identifiability.

3 Experimental and Real-world data analysis

To illustrate the methodology described in the previous sections, we conduct a series of experiments using both simulated and real-world data. The algorithm is implemented in Python version 3.10.12 and was executed on a desktop computer with an Intel Core i7-1300H processor and a 3.40 GHz clock speed. The code is available at <https://github.com/Dhorasso/smc2-seir-model>.

3.1 Experimental setup

We begin by applying the filtering algorithm to two synthetic datasets generated using the stochastic SEIR model introduced in Section 3. The simulation period spans $T = 100$ days, with a daily time step of $\delta t = 1$ day. The algorithm utilizes $N_\theta = 400$ parameter particles, $N_x = 200$ state particles, with $M = 5$ successive PMMH moves and a window size of $t_k = 20$ days. In Experiment 1, all model parameters remain constant, while Experiment 2 introduces a time-varying transmission rate. We assume that the data on daily new cases are the realization of a Poisson distribution: $y_t|x_t \sim \text{Poisson}(Y_{EI}(t))$, where $Y_{EI}(t)$ is the number of individual moving from E to I at time t .

3.1.1 Experiment 1

In this experiment, we assume constant parameters for the SEIR model: $\beta = 0.6$, $\sigma = \frac{1}{3}$, and $\gamma = \frac{1}{5}$. The total population size is $N = 6000$, with one initially infected individual. The latent state at time t is represented by $x_t = (S_t, E_t, I_t, R_t)$, and the parameters $\theta = (\beta, \sigma, \gamma)$ are to be estimated. The initial particle state vector in the O-SMC² algorithm is set to $(S_0, E_0, I_0, R_0) = (N - I_0, 0, I_0, 0)$, with I_0 drawn from a discrete uniform distribution, $I_0 \sim \mathcal{U}(0, \dots, 5)$. A uniform prior on the interval $[0, 1]$ is assigned to each of the parameters β , σ , and γ .

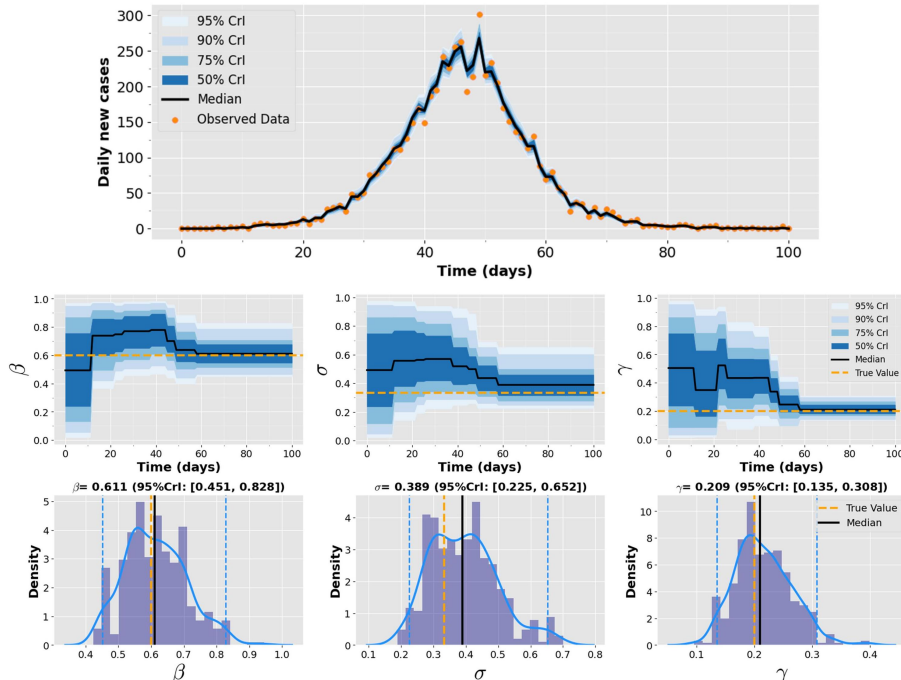


Fig. 4: State and parameter inference for Experiment 1. Top row: Filtering estimates of daily new infections, with observed values shown as orange dots. Middle row: Time series of filtering estimates for parameters β , σ , and γ . Bottom row: Posterior distributions of β , σ , and γ at the final time step, with 95% credible intervals in dashed blue lines. In rows 1 and 2, the solid black lines show the median estimate; shaded blue regions indicate posterior uncertainty quantiles. True parameter values are represented by orange dashed lines.

Figure 4 displays the sequential inference of daily new cases of infection together with the static parameters. We can observe that the predicted new cases are in good agreement with the data. The results also indicate that all true parameter values fall within the 95% credible interval, closely aligning with the posterior median as we evolve over time. Initially, during the epidemic's onset, the data lacks sufficient information within the time interval $[0, 20]$, resulting in widespread parameter uncertainty. However, as the epidemic approaches its peak, the inference algorithm captures the dynamics well, notably reducing parameter uncertainty. As the dynamics begin to slow around time $t = 60$, the posterior uncertainty stabilizes.

3.1.2 Experiment 2

In this experiment, we introduce variability in the transmission rate to simulate a more realistic scenario. Synthetic data are generated using a time-varying $\beta = \beta(t)$, modeled as:

$$\beta(t) = 0.3 \exp \left(\sin \left(\frac{2\pi t}{55} \right) - \frac{t}{80} \right), \quad (15)$$

while the parameters $\sigma = \frac{1}{2}$ and $\gamma = \frac{1}{7}$ remain constant. The total population size is $N = 200,000$, with five initially infected individuals. This experiment assesses the ability of the O-SMC² algorithm to capture state and static parameters under high transmission variability.

To accommodate the non-constant transmission rate, we model $\beta(t)$ in the model (1) as a geometric Brownian motion:

$$\beta(t) = e^{\log(\beta(t-1)) + \varepsilon_t}, \quad \varepsilon_t \sim \mathcal{N}(0, \nu_\beta^2), \quad (16)$$

where ν_β governs the variability in the transmission rate. The latent state vector is now $x_t = (S_t, E_t, I_t, R_t, \beta(t))$, and the parameters to estimate are $\theta = (\sigma, \gamma, \nu_\beta)$. The O-SMC² algorithm uses the same initial particle state as in Experiment 1, with $\beta(0) \sim \mathcal{U}(0.2, 0.5)$.

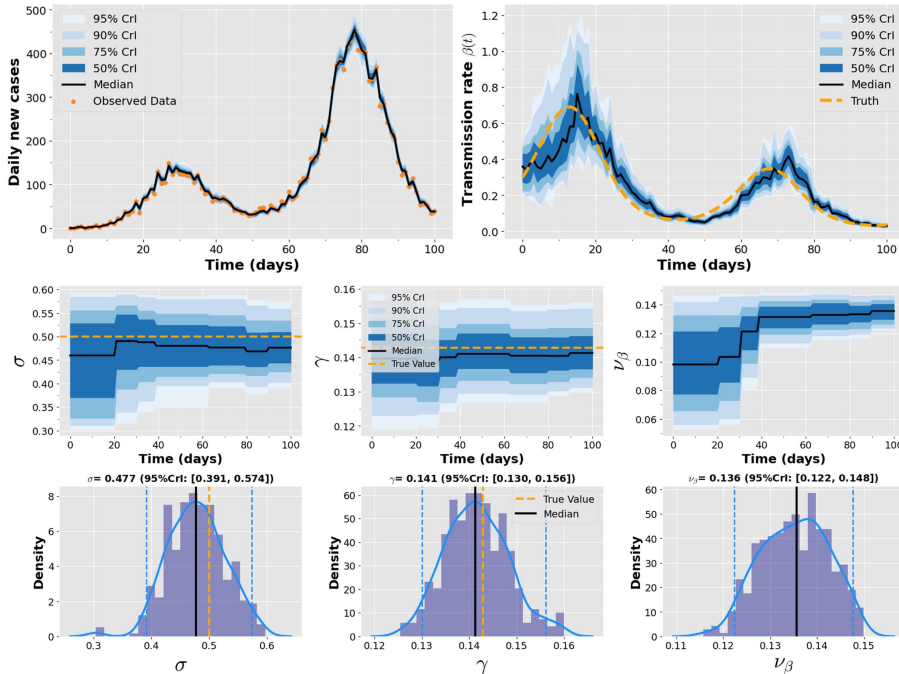


Fig. 5: State and parameter inference for Experiment 2. Top row: Left - Filtering estimates of daily new infections with observed values in orange; Right - Filtering estimate of the time-dependent transmission rate $\beta(t)$. Middle row: Filtering estimates of σ , γ , and ν_β over time. Bottom row: Posterior distributions of σ , γ , and ν_β the final time step, with 95% credible intervals in dashed blue lines. In rows 1 and 2, the solid black lines show the median estimate; shaded blue regions indicate posterior uncertainty quantiles. True parameter values are represented by orange dashed lines.

Priors for the parameters are $\sigma \sim \mathcal{U}(0.3, 0.6)$, $\gamma \sim \mathcal{T}\mathcal{N}_{[0,1]}(0.14, 0.01)$, and $\nu_\beta \sim \mathcal{T}\mathcal{N}_{[0.05, 0.15]}(0.1, 0.05)$. A more restrictive prior on γ is used due to its high correlation with the transmission rate $\beta(t)$, especially during abrupt changes in transmission dynamics. Fluctuations in new cases can reflect changes in $\beta(t)$, but could also be influenced by γ as shown in (Inouzhe et al., 2023). The prior for ν_β allows for rapid changes in the transmission rate, ensuring the model can adapt to sudden shifts in disease dynamics and aligns with values observed in the literature (Funk et al., 2018; Calvetti et al., 2021).

Figure 5 demonstrates the ability of the method to track multiple outbreak waves and capture the trend in a time-varying transmission rate, albeit with a minor lag. This slight delay is expected, as the analysis relies on daily case data (i.e., the number of newly infectious individuals transitioning from E to I) rather than exact counts of new infections (i.e., individuals moving from S to E), which are often unknown during an epidemic. As with Experiment 1, the true parameter values lie within the 95% credible interval, indicating reliable parameter estimation even under conditions of variable transmission.

To evaluate the performance of the O-SMC² algorithm, we tested a range of window sizes t_k , keeping the priors and number of particle configurations consistent across experiments. Tables 2 and 3 in Appendix C show that even with smaller window sizes, the algorithm produces reasonable parameter estimates that are close to the true values, with credible intervals comparable to those of standard SMC² approach (i.e., when all past observations are used at each time step), although slightly larger for smaller window sizes. Notably, the computational cost decreases substantially with smaller windows, making O-SMC² well-suited for real-time or resource-limited settings. These findings align with previous research (Vieira (2018), Chapter 15). Figures 1-2 in Appendix C display the posterior densities of the parameters at the final time step, demonstrating consistency with estimates obtained using SMC².

3.2 Real case study: Analysis of COVID-19 in Ireland

Since the onset of the COVID-19 pandemic in December 2019 in Wuhan, China, the World Health Organization (WHO) has reported over 772 million confirmed cases globally and more than 69 million deaths (World Health Organisation (WHO), 2024). The rapid transmission and widespread nature of the virus led the WHO to declare it a pandemic. In Cazelles et al. (2021), particle MCMC has been employed to reconstruct the COVID-19 epidemic's trajectory in Ireland. However, it is worth noting that while this method efficiently tracks observed data, it remains an offline approach and may not be suitable for real-time decision-making when rapid responses are required.

3.2.1 Model

We present a fully discrete stochastic extended-SEIR model to study the spread of COVID-19, with a structure designed to capture changes in transmission dynamics during the pandemic. In this model, individuals transition through compartments representing different stages of infection: S_t representing susceptible individuals, E_t for those who are exposed and infected but not yet infectious, A_t for asymptomatic infectious individuals, I_t for symptomatic infectious individuals, and finally, R_t is the number of individuals recovering or succumbing to the virus. The following discrete equations describe the dynamics of the model:

$$\begin{aligned} S_{t+\delta t} &= S_t - Y_{SE}(t), \\ E_{t+\delta t} &= E_t + Y_{SE}(t) - Y_E(t), \\ A_{t+\delta t} &= A_t + Y_{EA}(t) - Y_{AR}(t), \\ I_{t+\delta t} &= I_t + Y_E(t) - Y_{EA}(t) - Y_{IR}(t), \\ R_{t+\delta t} &= R_t + Y_{AR}(t) + Y_{IR}(t), \end{aligned} \tag{17}$$

where $Y_{AB}(t)$ represents the number of individuals moving from compartment A to compartment B at time t and these quantities are defined through the binomial random variables:

$$\begin{aligned} Y_{SE}(t) &\sim \text{Bin}\left(S_t, 1 - \exp\left(-\beta(t) \frac{(I_t + r_A A_t)}{N} \delta t\right)\right), \\ Y_E(t) &\sim \text{Bin}\left(E_t, 1 - e^{-\sigma \delta t}\right), \quad Y_{EA}(t) \sim \text{Bin}(Y_E(t), p_A), \\ Y_{AR}(t) &\sim \text{Bin}\left(A_t, 1 - e^{-\gamma \delta t}\right), \quad Y_{IR}(t) \sim \text{Bin}\left(I_t, 1 - e^{-\gamma \delta t}\right). \end{aligned} \quad (18)$$

The model assumes a homogeneously mixing population of constant size:

$$N = S_t + E_t + A_t + I_t + R_t. \quad (19)$$

The models presented in (17)-(18), do not explicitly incorporate vaccination. This is because they are primarily designed to focus on the spread of the virus and the impact of various non-pharmaceutical interventions during a period when vaccines are either unavailable or not yet widely deployed. However, the effect of vaccination can easily be introduced by adding a compartment for vaccinated individuals and adjusting the transmission dynamics to reflect partial or complete immunity. Allowing the transmission rate to be time-varying seems reasonable since, throughout the epidemic, the intensity of disease transmission will tend to vary due to individuals' behavioral changes or government lockdown measures. Hence, we consider a geometric random walk (RW) model for the transmission rate:

$$\beta(t) = e^{\log(\beta(t-1)) + w_t}, \quad w_t \sim \mathcal{N}(0, \nu_\beta^2), \quad (20)$$

where ν_β is the parameter controlling the innovation in the transmission rate, consistent with previous study of COVID-19 in Ireland (Cazelles et al., 2021). Giving the distribution of $\beta(t)$, we can sequentially estimate the distribution of the effective reproduction number ($R_{\text{eff}}(t)$) that refers to the average number of secondary infections caused by a single infected individual during their infectious period in a population where some individuals are immune or other interventions have been implemented:

$$R_{\text{eff}}(t) = \beta(t) \left(\frac{(1 - p_A) + p_A r_A}{\gamma} \right) \frac{S_t}{N}. \quad (21)$$

In general, when $R_{\text{eff}}(t) > 1$, the number of observed cases will increase, while it will decrease if $R_{\text{eff}}(t) < 1$. Consequently, policymakers can determine whether to relax or strengthen control measures based on whether R_{eff} falls below the self-sustaining threshold of 1.

3.2.2 Data and model fitting

The data we use are daily confirmed case counts extracted from an up-to-date database of the Irish Health Protection Surveillance Centre (HPSC) (<https://COVID19ireland-geohive.hub.arcgis.com/>). To integrate these observations into our model, we define the variable: C_t^I representing the cumulative number of infectious cases. This variable evolves according to the equation:

$$C_{t+1}^I = C_t^I + Y_E(t) - Y_{EA}(t). \quad (22)$$

Hence, $\mu_t = C_{t+1}^I - C_t^I$ represents the daily expected number of cases. Since daily reported case counts are subject to observation error and typically exhibit overdispersion (where the conditional variance exceeds the conditional mean), we model the observed daily cases, Z_t^I , using a normal approximation of the negative binomial distribution (chosen for computational efficiency, Funk et al. (2018)). The negative binomial distribution is a generalization of the Poisson distribution that can account for overdispersion in count data. Specifically,

for the negative binomial distribution, the mean is μ_t and the variance is $\mu_t(1+\phi\mu_t)$, where ϕ is an overdispersion parameter. To avoid singularities when $\mu_t = 0$, we followed the approach of [Funk et al. \(2018\)](#), rounding variances smaller than 1 up to 1. The observed daily case counts follow a negative binomial distribution:

$$Z_t^I \sim \mathcal{N}(\mu_t, \mu_t(1+\phi\mu_t)). \quad (23)$$

We estimate the spread of COVID-19 in Ireland from February 29th, 2020, to February 28th, 2021, using the daily new case count data over 365 days. The Irish population in 2020 was estimated to be $N = 4,965,439$. The O-SMC² uses $N_\theta = 1000$ parameter particles, $N_x = 500$ state particles, $M = 5$ successive PMMH moves and a window size of $t_k = 80$ days. Table 1 in Appendix D gives the description and prior of the inferred parameters used in the model (18). These priors are based on previous studies of COVID-19 dynamics in Ireland ([Irish Department of Health, 2020](#); [Cazelles et al., 2021](#)). For the choice of prior distributions for the hyperparameters, ν_β (which governs the variability in the transmission rate) and ϕ (the overdispersion parameter), we adopt settings that allow for rapid changes in the transmission rate, ensuring the model can adapt to sudden shifts in disease dynamics, as discussed in ([Funk et al., 2018](#)). Regarding initial states, we set: $S_0 = N - E_0 - A_0$, $E_0 = 1$, $A_0 \sim \mathcal{U}(\{10, \dots, 50\})$ and $I_0 = R_0 = 0$. The execution time for the 365 days considered here was less than 5 hours, making it suitable for practical real-time applications.

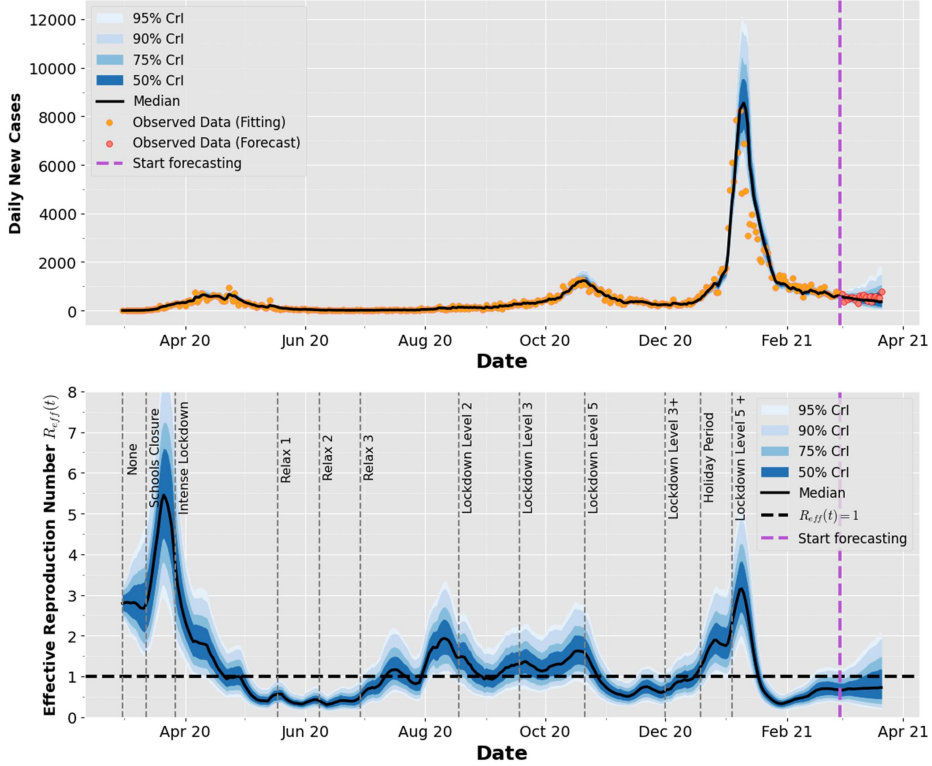


Fig. 6: Model fitting with COVID-19 data in Ireland. The top row shows the estimated daily number of new cases. The observed data used for model fitting are shown as orange dots, while the red dots represent observed data that were excluded from fitting and used solely for forecast validation. The bottom row presents the weekly average of the time-dependent effective reproduction number. The solid black lines show the median estimate; shaded blue regions indicate posterior uncertainty quantiles. The vertical grey dashed lines represent the different government interventions. The vertical dashed violet line marks the last date of observations, beyond which the model is used to forecast the next 21 days.

Figure 6 illustrates the model's fit to the daily number of COVID-19 cases reported in Ireland. The top plot shows the daily new cases, with three noticeable peaks: one in

mid-April 2020, another in mid-November 2020, and a larger peak in early January 2021. The model successfully captures these three waves, with observed data (orange dots) falling within the 95% credible interval on most days. The fitting period achieved a mean absolute error (MAE) of 139.59 and a continuous ranked probability score (CRPS) of 105.78. These evaluation metrics are defined in detail in Appendix D. However, a sudden drop in reported cases around mid-January 2021 is not fully captured, likely due to real-world factors such as reporting delays or testing changes not included in the model. Beyond February 28th, 2021, the model projects cases forward for 21 days, excluding data from April 1 (red dots) from the fitting process. The forecast period shows good predictive accuracy with an MAE of 113.71 and a CRPS of 98.45, and the observed data fall within the 95% credible interval, indicating strong agreement between predictions and actual trends.

The bottom plot in Figure 6 shows the weekly-averaged effective reproduction number, $R_{\text{eff}}(t)$, with corresponding daily estimates (not averaged) presented in Figure 1 in Appendix D. As anticipated, $R_{\text{eff}}(t)$ fluctuates in response to changes in the epidemic dynamics. The impact of the first lockdown is clearly evident, as it drives $R_{\text{eff}}(t)$ below one, effectively ending the first wave. A gradual increase in $R_{\text{eff}}(t)$ occurred in June 2020, due to the easing of restrictions. $R_{\text{eff}}(t)$ remained above one until mid-October, corresponding to the second wave of the epidemic. The second round of lockdown measures caused $R_{\text{eff}}(t)$ to decline by November 2020, falling below one once more. The emergence of the more transmissible Alpha variant, combined with increased social interactions during the holiday season, resulted in a sharp rise in cases toward the end of 2020. This was followed by a third round of lockdown measures, which once again brought $R_{\text{eff}}(t)$ below one (see the supplementary material of [Jaouimaa et al. \(2021\)](#) for a description of the individual lockdown measures).

In Figure 7, we present the sequential estimation of the parameters of model (17) over 365 days of the pandemic. The graphs display the posterior medians of the parameters, accompanied by their respective uncertainty intervals at each time step. The posterior distributions of the parameters obtained at the final time step (see Table 1 in Appendix D) are aligned with the results found in [Cazelles et al. \(2021\)](#) using PMCMC methods.

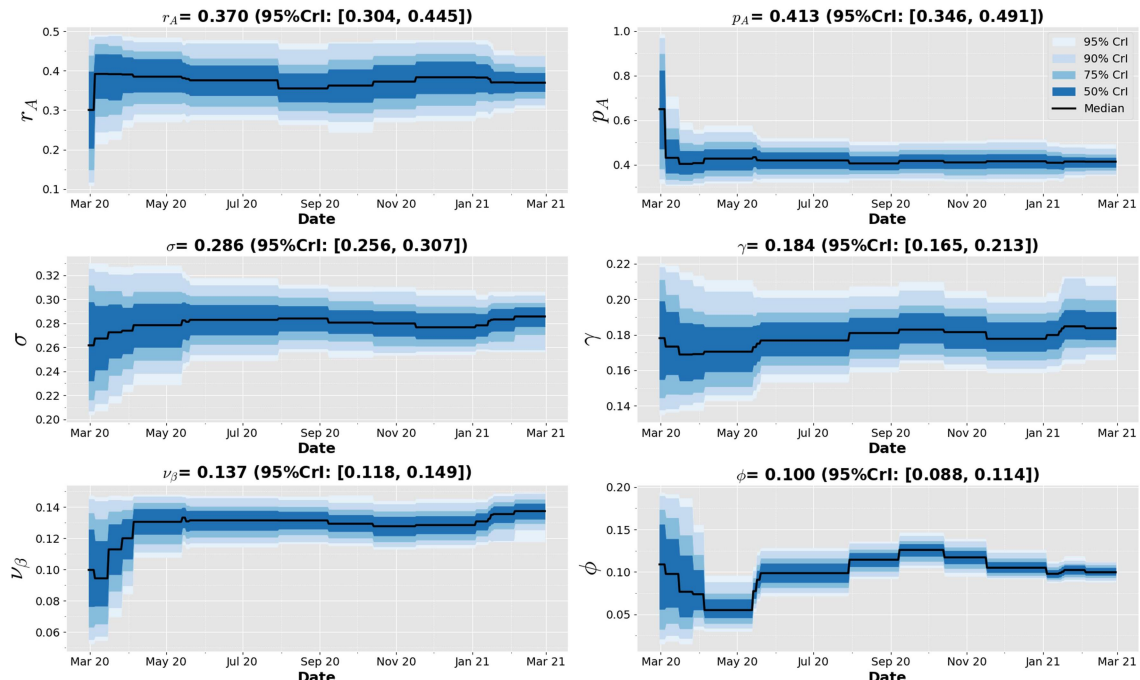


Fig. 7: Filtered estimate of the parameter in the COVID-19 model using O-SMC² algorithm. The solid black lines represent the median estimate; shaded blue regions indicate posterior uncertainty quantiles.

Figure 1 in Appendix E illustrates the application of the O-SMC² for real-time monitoring, using partial datasets spanning four distinct time periods: February 29, 2020, to May 30, 2020; May 30, 2020, to August 29, 2020; August 29, 2020, to November 28, 2020; and November 28, 2020, to February 27, 2021. At each stage, the algorithm utilizes the results from the previous O-SMC² run as prior information to compute the joint posterior $p(x_{i:j}, \theta | y_{i:j})$. This sequential approach enables the efficient integration of new data while maintaining computational efficiency. Moreover, it significantly improves the methodology described in Dureau et al. (2013), which relied on PMCMC and required the model to be rerun from scratch for each new batch of data.

4 Conclusion

In this paper, we explored the application of an online variant of the Sequential Monte Carlo Squared (O-SMC²) method for real-time inference in stochastic epidemic models. This approach differs from standard SMC² by integrating a mechanism that approximates the posterior distribution using a fixed window of recent observations, thereby reducing computational demands while maintaining parameter estimation accuracy. This adaptation makes O-SMC² particularly suitable for dynamic disease modeling, where timely responses are critical. We demonstrated the effectiveness of O-SMC² in the stochastic SEIR compartment model, validating its performance on both synthetic simulations and real-world COVID-19 data from Ireland. Our results show that O-SMC², even with a modest window size, effectively tracks epidemic progression and generates robust online estimates of both static and dynamic epidemiological parameters. Moreover, the sequential nature of this method enables the efficient updating of estimates by using results from previous runs as prior information, eliminating the need to rerun the model from scratch as new data becomes available incrementally. This feature underscores the practicality of O-SMC² for real-time epidemiological surveillance, informing public health authorities on adaptation of interventions based on real-time information assimilation. However, we also acknowledge certain challenges, particularly in the early stages of an outbreak when available data may be sparse and less informative. During this phase, prior uncertainty, potential parameter non-identifiability, and low case counts can collectively reduce the reliability of estimates. These issues can result in wide credible intervals and greater variability in posterior distributions. One practical consideration is the choice of the fixed window size, t_k , which impacts the balance between computational efficiency and the informativeness of the data used for inference. In our experiments, setting t_k to approximately 20% of the total time series length provided a reasonable compromise. However, in truly online settings, where data arrives as a continuous stream without a predetermined end, a fixed window size may not be optimal. An adaptive strategy that dynamically adjusts t_k , for example, by increasing the window size when the PMMH acceptance rate fall below a certain threshold, could improve the robustness during periods of rapid change or less informative observations. Exploring such adaptive mechanisms and integrating more flexible modeling approaches are key directions for enhancing the responsiveness and reliability of early-stage inference in real-time epidemic monitoring.

Acknowledgements

This publication has emanated from research conducted with the financial support of Taighde Éireann – Research Ireland under Grant number 21/FFP-P/10123. We wish to thank the editor and the anonymous reviewers for their constructive comments and suggestions which greatly improved the quality of this paper.

A Structural identifiability analysis

To assess structural identifiability, we first derived a deterministic mean-field approximation of the stochastic SEIR model. This step is necessary because most identifiability analysis tools require a system of ordinary differential equations (ODEs) as input. Starting from the discrete-time stochastic model, we replaced each binomial transition with its expected value and applied the first-order approximation $1 - e^{-x} \approx x$ for $x \ll 1$. Taking the limit as $\delta t \rightarrow 0$, we obtained the following system:

$$\frac{dS}{dt} = -\beta \frac{SI}{N}, \quad \frac{dE}{dt} = \beta \frac{SI}{N} - \sigma E, \quad \frac{dI}{dt} = \sigma E - \gamma I, \quad \frac{dR}{dt} = \gamma I. \quad (24)$$

We assumed the observable is $y_1(t) = \sigma E(t)$, representing daily new infections. All parameters are also assumed to be static throughout the analysis, consistent with standard structural identifiability frameworks.

Structural identifiability refers to the theoretical ability to uniquely recover model parameters from perfect data, given the model structure and observables. This was assessed using the Julia package `StructuralIdentifiability.jl` (Dong et al., 2023). The total population size N and the initial conditions were assumed to be known during the analysis. Results (Table 1) show that for both the standard SEIR and the SEAIR model, key parameters such as β , σ , γ and additional parameters in the extended model, are structurally globally identifiable. For the SEIR model, we also found that all parameters remain globally identifiable even when the initial conditions are unknown, provided that N is known. These findings confirm that the selected observables are theoretically sufficient to uniquely identify the parameters prior to applying the O-SMC² algorithm. For a tutorial introduction to `StructuralIdentifiability.jl` in epidemic modeling, see (Liyanage et al., 2025).

Tab. 1: Structural identifiability results.

SEIR	SEAIR
<pre> julia> ode = @ODEmodel(S'(t) = - beta*S(t)*I(t)/N, E'(t) = beta*S(t)*I(t)/N - sigma*E(t), I'(t) = sigma*E(t) - gamma*I(t), R'(t) = gamma*I(t), y1(t) = sigma*E(t), y2(t) = N) julia> assess_identifiability(ode, known_ic = [S,E,I,R]) S(0) => :globally E(0) => :globally I(0) => :globally R(0) => :globally beta => :globally gamma => :globally sigma => :globally </pre>	<pre> julia> ode = @ODEmodel(S'(t) = - beta*S(t)*(I(t)+ra*A(t))/N, E'(t) = beta*S(t)*(I(t)+ra*A(t))/N - sigma*E(t), A'(t) = pa*sigma*E(t) - gamma*A(t), I'(t) = (1-pa)*sigma*E(t) - gamma*I(t), R'(t) = gamma*A(t) + gamma*I(t), y1(t) = (1-pa)*sigma*E(t), y2(t) = N) julia> assess_identifiability(ode, known_ic = [S,E,A,I,R]) S(0) => :globally E(0) => :globally A(0) => :globally I(0) => :globally R(0) => :globally N => :globally beta => :globally gamma => :globally pa => :globally ra => :globally sigma => :globally </pre>

B Approximation of the acceptance probability

During the rejuvenation step in the algorithm 2, when a new parameter θ^* is proposed at time t , an unbiased estimate of the marginal likelihood is computed by running Algorithm 1 over observations from time 1 to t . However, as time progresses, the computational cost of this procedure grows, making it less feasible for long-time series data. This limitation can be alleviated by considering only the most recent observations (Vieira, 2018).

Let the window size be denoted by $t_k > 0$. By the law of total probability, the marginal

likelihood at time t can be factorized as:

$$\begin{aligned} p(y_{1:t}|\theta) &= \left(\prod_{s=1}^{t-t_k} p(y_s|y_{1:s-1}, \theta) \right) \times \left(\prod_{s=t-t_k+1}^t p(y_s|y_{1:s-1}, \theta) \right) \\ &= p(y_{1:t-t_k}|\theta) \times \left(\prod_{s=t-t_k+1}^t p(y_s|y_{1:s-1}, \theta) \right). \end{aligned} \quad (25)$$

For $s \geq t - t_k$, if we assume that for a sufficiently large t_k , the older observations $y_{1:t-t_k}$ have minimal impact on the filtering estimate of the latent state at time $s - 1$, i.e., $p(x_{s-1}|y_{1:s-1}, \theta) \approx p(x_{s-1}|y_{t-t_k+1:s-1}, \theta)$, then, from the result in (Kantas et al., 2015), we have:

$$\begin{aligned} p(y_s|y_{1:s-1}, \theta) &= \int g(y_s|x_s, \theta) f(x_s|x_{s-1}, \theta) p(x_{s-1}|y_{1:s-1}, \theta) dx_{s-1:s} \\ &\approx \int g(y_s|x_s, \theta) f(x_s|x_{s-1}, \theta) p(x_{s-1}|y_{t-t_k+1:s-1}, \theta) dx_{s-1:s} \\ &= p(y_s|y_{t-t_k+1:s-1}, \theta). \end{aligned} \quad (26)$$

This approximation yields to:

$$p(y_{1:t}|\theta) \approx p(y_{1:t-t_k}|\theta) \times p(y_{t-t_k+1:t}|\theta), \quad (27)$$

with:

$$p(y_{t-t_k+1:t}|\theta) = \prod_{s=t-t_k+1}^t p(y_s|y_{t-t_k+1:s-1}, \theta) \approx \prod_{s=t-t_k+1}^t p(y_s|y_{1:s-1}, \theta). \quad (28)$$

Given the current θ -particle, the new parameter θ^* at time t is drawn from the region where most of the probability mass is located (Chopin, 2002). Under the assumption that the target parameter vector remains constant over time, and provided that the window size t_k is large enough to capture the necessary temporal variability in the observations $y_{t-t_k+1:t}$, it is reasonable to assume that the historical likelihoods $p(y_{1:t-t_k}|\theta)$ and $p(y_{1:t-t_k}|\theta^*)$ are approximately equal. Consequently, their contribution to the likelihood ratio becomes negligible. Under this assumption, the full likelihood ratio simplifies to:

$$\frac{p(y_{1:t}|\theta^*)}{p(y_{1:t}|\theta)} \approx \frac{p(y_{t-t_k+1:t}|\theta^*)}{p(y_{t-t_k+1:t}|\theta)}. \quad (29)$$

Thus, using the SMC estimate of the incremental likelihood for a fixed number of particles N_x (see Equation (8)), we estimate the windowed likelihood $p(y_{t-t_k+1:t}|\theta)$ as:

$$\hat{p}_{N_x}(y_{t-t_k+1:t}|\theta) = \prod_{s=t-t_k+1}^t \left(\frac{1}{N_x} \sum_{i=1}^{N_x} w_s^i(x_{s-1}^i, x_s^i) \right), \quad (30)$$

and the acceptance probability for the PMMH kernel is given by:

$$\alpha = \min \left\{ 1, \frac{\hat{p}_{N_x}(y_{t-t_k+1:t}|\theta^*) p(\theta^*)}{\hat{p}_{N_x}(y_{t-t_k+1:t}|\theta) p(\theta)} \times \frac{q(\theta|\theta^*)}{q(\theta^*|\theta)} \right\}. \quad (31)$$

C Posterior estimate in the simulation study

Here, we present the posterior estimates of model parameters from two experimental setups using the O-SMC² algorithm. The experiments test varying window sizes t_k to evaluate the computational efficiency and the impact of window length on parameter inference.

Table 1 summarizes the parameter settings and prior distributions used in the two simulation experiments. For each window size, we report the posterior median and 95% credible intervals, comparing them to SMC² estimates to assess both inference accuracy and computational savings. Tables 2 and 3 display these results for Experiments 1 and 2, respectively, including the “Relative Efficiency” defined as the ratio of the SMC² computational time to the O-SMC² computational time. This metric quantifies the time reduction achieved by O-SMC² for each t_k compared to SMC², with larger ratios indicating greater computational efficiency.

Tab. 1: Summary of parameter settings used in the two simulation Experiments. $\mathcal{U}(\text{inf}, \text{sup})$ indicates a uniform distribution and \mathcal{TN} stands for truncated normal distribution ($\mathcal{TN}_{[\text{inf}, \text{sup}]}(\text{mean}, \text{std})$).

Parameter	Description	Value in simulation	Prior	Notes
Experiment 1				
β	Transmission rate	0.6	$\mathcal{U}(0, 1)$	Estimated
σ	Rate from exposed to infectious	1/3	$\mathcal{U}(0, 1)$	Estimated
γ	Recovery rate	1/5	$\mathcal{U}(0, 1)$	Estimated
I_0	Initial infected individuals	1	$\mathcal{U}(\{0, \dots, 5\})$	—
N	Population size	6000	—	Fixed
Experiment 2				
$\beta(t)$	Time-varying transmission rate	$\beta(t) = 0.3 \exp(\sin(\frac{2\pi t}{55}) - \frac{t}{80})$	Modeled via Eq. (16)	Estimated
σ	Rate from exposed to infectious	1/2	$\mathcal{U}(0.3, 0.6)$	Estimated
γ	Recovery rate	1/7	$\mathcal{TN}_{[0,1]}(0.14, 0.01)$	Estimated
ν_β	Volatility in $\beta(t)$	—	$\mathcal{TN}_{[0.05, 0.15]}(0.1, 0.05)$	Estimated
$\beta(0)$	Initial transmission rate	0.3	$\mathcal{U}(0.2, 0.5)$	—
I_0	Initial infected individuals	5	$\mathcal{U}(\{0, \dots, 5\})$	—
N	Population size	200,000	—	Fixed

Tab. 2: Summary of parameter estimates in Experiment 1. Posterior medians and 95% credible intervals were obtained using O-SMC² with varying window sizes t_k at the final time step $T = 100$. “Relative Efficiency” denotes the factor by which computational time is reduced compared to SMC².

t_k	β	σ	γ	Relative Efficiency
20	0.611 (0.4751, 0.828)	0.389 (0.225, 0.652)	0.209 (0.135, 0.308)	1.70
40	0.603 (0.442, 0.870)	0.367 (0.219, 0.562)	0.213 (0.127, 0.338)	1.18
60	0.639 (0.499, 0.847)	0.334 (0.235, 0.447)	0.228 (0.158, 0.329)	1.10
80	0.638 (0.496, 0.845)	0.336 (0.235, 0.479)	0.224 (0.158, 0.325)	1.02
SMC ²	0.612 (0.470, 0.809)	0.325 (0.236, 0.468)	0.208 (0.148, 0.305)	-
Truth	0.6	0.333	0.2	-

Tab. 3: Summary of parameter estimates in Experiment 2. Posterior medians and 95% credible intervals were obtained using O-SMC² with varying window sizes t_k at the final time step $T = 100$. “Relative Efficiency” denotes the factor by which computational time is reduced compared to SMC².

t_k	σ	γ	ν_β	Relative Efficiency
20	0.477 (0.391, 0.574)	0.141 (0.130, 0.156)	0.136 (0.122, 0.148)	3.22
40	0.479 (0.391, 0.573)	0.141 (0.128, 0.154)	0.138 (0.125, 0.149)	1.59
60	0.476 (0.393, 0.571)	0.141 (0.132, 0.150)	0.139 (0.126, 0.149)	1.29
80	0.475 (0.387, 0.576)	0.142 (0.131, 0.154)	0.140 (0.127, 0.149)	1.06
SMC ²	0.491 (0.406, 0.588)	0.143 (0.134, 0.153)	0.139 (0.127, 0.149)	-
Truth	0.5	0.142	-	-

While smaller t_k values yield significant computational savings, this efficiency advantage decreases as t_k increases. For most tested window sizes, the credible intervals align closely with those from SMC², indicating minimal bias in this application. However, smaller windows may introduce minor biases if the window does not capture sufficient temporal dependencies, potentially resulting in slightly larger 95% credible intervals (Figures 1-2).

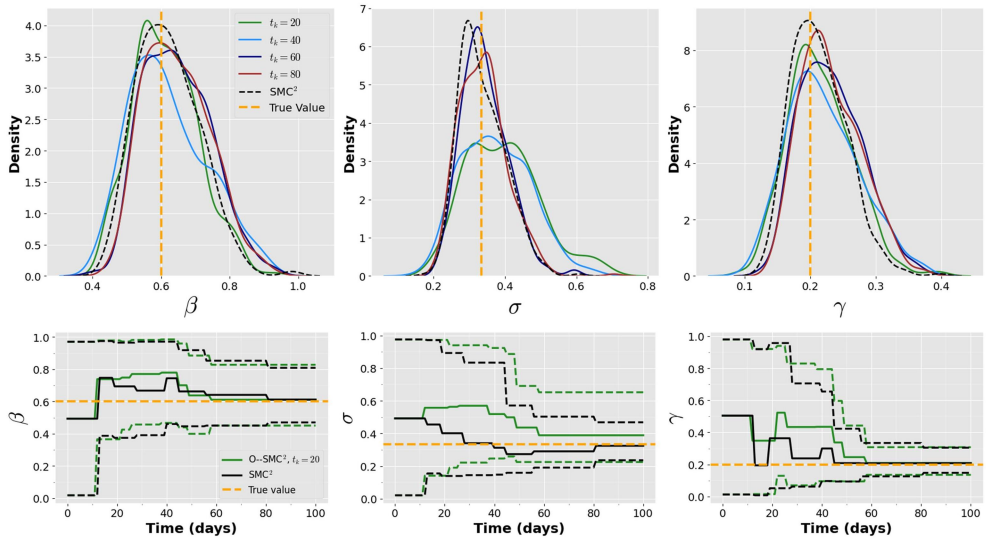


Fig. 1: Posterior densities of parameters at $T = 100$ (top) and filtered estimates (bottom) in Experiment 1. The dashed lines in the bottom plot indicate the 95% credible intervals. True parameter values are represented by orange dashed lines.

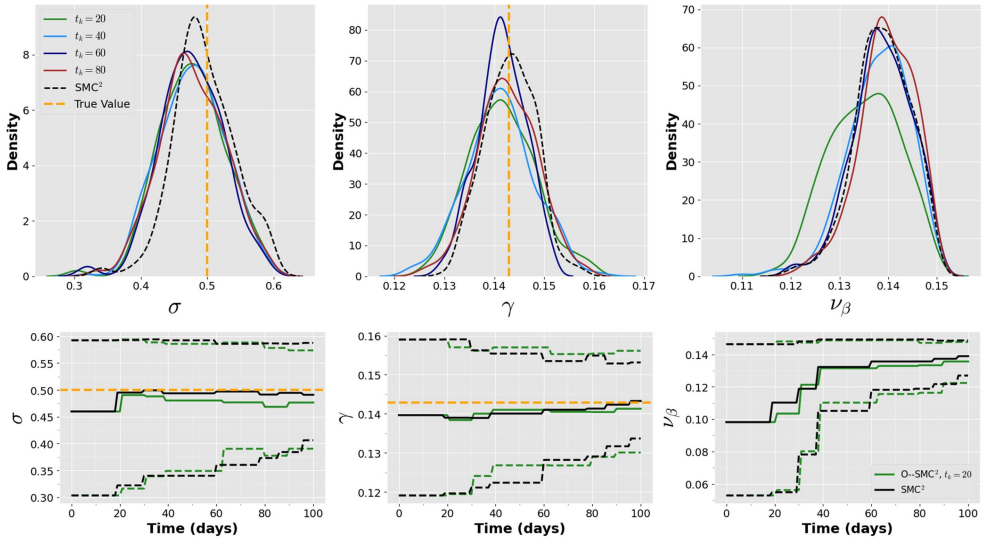


Fig. 2: Posterior densities of parameters at $T = 100$ (top) and filtered estimates (bottom) in Experiment 2. The dashed lines in the bottom plot indicate the 95% credible intervals. True parameter values are represented by orange dashed lines.

It is important to note that the windowing mechanism is applied only during the resampling step (i.e., when ESS drops below 50% of the total number of parameter particles in our case). Thus, the greater the frequency of resampling at time t (especially when t is significantly larger than t_k), the more computationally beneficial O-SMC² becomes. In Figure 3, we observe that the frequency of resampling at times well beyond $t_k = 20$ gradually decreases in Experiment 1, while it remains more frequent in Experiment 2. This explains the greater computational gain observed in Experiment 2.

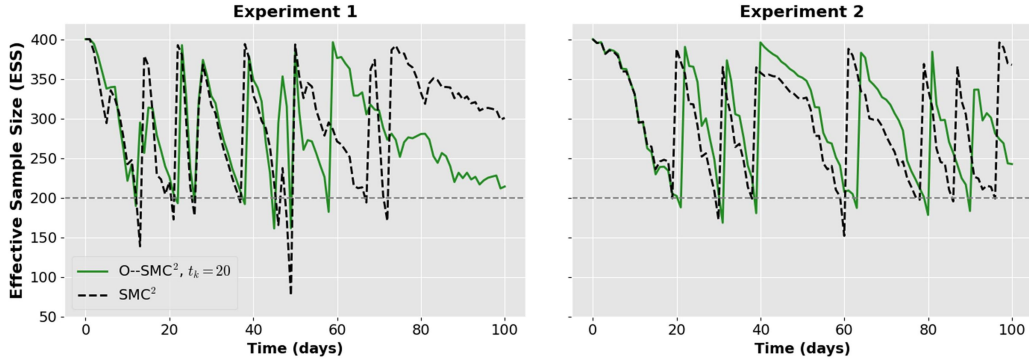


Fig. 3: Effective Sample Size. The left graph shows the evolution of the ESS in Experiment 1 and the right one the evolution in Experiment 2.

D Parameter settings in the COVID-19 model

Table 1 summarizes parameters from the COVID-19 model (Equation (17)), including hyperparameters (Equations (20) and (23)). For each parameter, prior and posterior estimates (median and 95% credible interval) are provided. Priors were informed by COVID-19 dynamics literature in Ireland (Irish Department of Health, 2020; Cazelles et al., 2021).

Tab. 1: Description of the different parameters, priors and posteriors estimate at the final time $T = 365$ days. Upper bound and/or lower bound have been imposed by the observations. \mathcal{TN} stands for truncated normal distribution ($\mathcal{TN}_{[\text{inf}, \text{sup}]}(\text{mean}, \text{std})$).

Parameter	Description	Prior value	Posterior median (95% CrI)
r_A	Reduction factor of transmission from A_t	$\mathcal{U}(0.1, 0.5)$	0.370 (0.304, 0.445)
p_A	Fraction of infected asymptomatic cases	$\mathcal{U}(0.3, 1)$	0.413 (0.313, 0.491)
$\beta(0)$	Initial condition transmission rate	$\mathcal{U}(0.6, 0.8)$	-
σ	Rate from exposed to infectious	$\mathcal{TN}_{[1/3, 1/5]}(1/4, 0.1)$	0.286 (0.256, 0.307)
γ	Removal rate	$\mathcal{TN}_{[1/7.5, 1/4.5]}(1/6, 0.2)$	0.184 (0.165, 0.213)
ν_β	Volatility of the Brownian process	$\mathcal{TN}_{[0.05, 15]}(0.1, 0.05)$	0.137 (0.118, 0.149)
ϕ	Overdispersion	$\mathcal{U}(0.01, 0.2)$	0.100 (0.088, 0.114)

To evaluate predictive accuracy, we report the Mean Absolute Error (MAE) and the Continuous Ranked Probability Score (CRPS).

The MAE quantifies the average absolute deviation between the observed values and the model's predictive mean:

$$\text{MAE} = \frac{1}{T} \sum_{t=1}^T |y_t - \hat{\Delta}_t| \quad (32)$$

where y_t is the true value of the incidence at time t , and $\hat{\Delta}_t = \text{E}[\Delta_t | y_{1:t}]$ is the model posterior predictive mean of the incidence.

The CRPS evaluates the quality of the full predictive distribution by comparing the predicted cumulative distribution function (CDF) to the empirical CDF of the observation:

$$\text{CRPS} = \frac{1}{T} \sum_{t=1}^T \int_{-\infty}^{\infty} (F_t(u) - \mathbb{I}(y_t \leq u))^2 du$$

where $F_t(u) = p(\Delta_t \leq u | y_{1:T})$ is the predictive CDF at time t , and $\mathbb{I}(\cdot)$ is the indicator function.

When the predictive distribution is represented by a set of particles $\{x_t^i\}_{i=1}^{N_x}$, the CRPS

can be approximated as:

$$\text{CRPS} \approx \frac{1}{T} \sum_{t=1}^T \left(\frac{1}{N_x} \sum_{i=1}^{N_x} |y_t - x_t^i| - \frac{1}{2N_x^2} \sum_{i=1}^{N_x} \sum_{j=1}^{N_x} |x_t^i - x_t^j| \right)$$

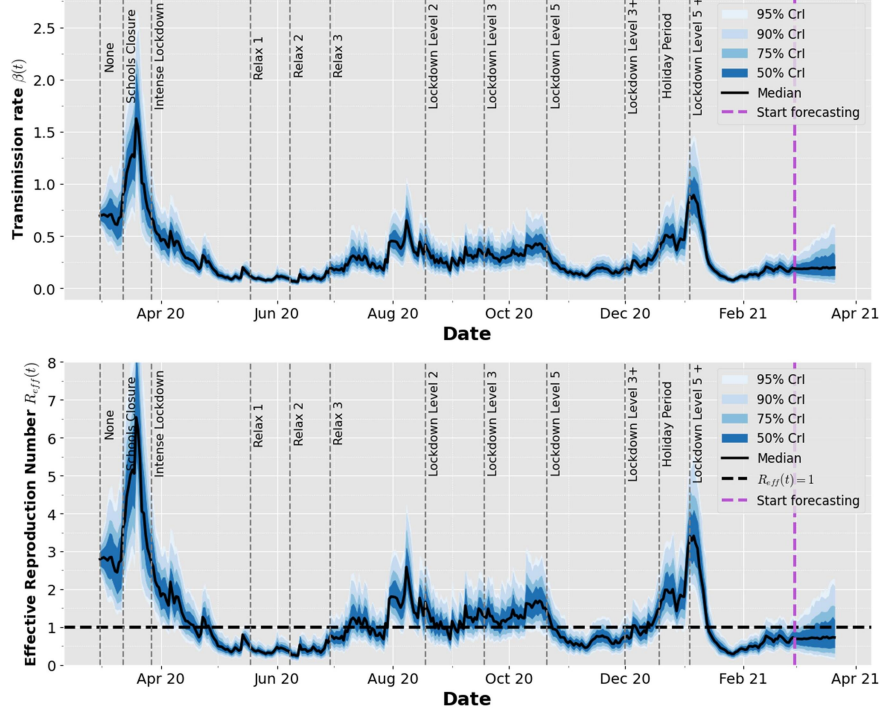


Fig. 1: Daily estimates of the time-dependent transmission rate and effective reproduction number. The solid black lines represent the median estimate of $R_{\text{eff}}(t)$, with shaded blue regions indicating posterior uncertainty quantiles. Weekly averaged estimates of $R_{\text{eff}}(t)$ are shown in Figure 6.

E Application in real-time surveillance

The methodology developed in this paper is applied to a real-time surveillance setting, demonstrating how our model can track evolving dynamics in sequential data. By integrating new observations over time, the model provides insights into the system's behavior. The focus is on an adaptive framework that updates the posterior distribution, conditioned on incoming data, while utilizing results from previous O-SMC² runs as prior information. The results are shown in Figure 1, where we observe that there is no significant difference compared to the results obtained from running the model from scratch (see Figure 6).

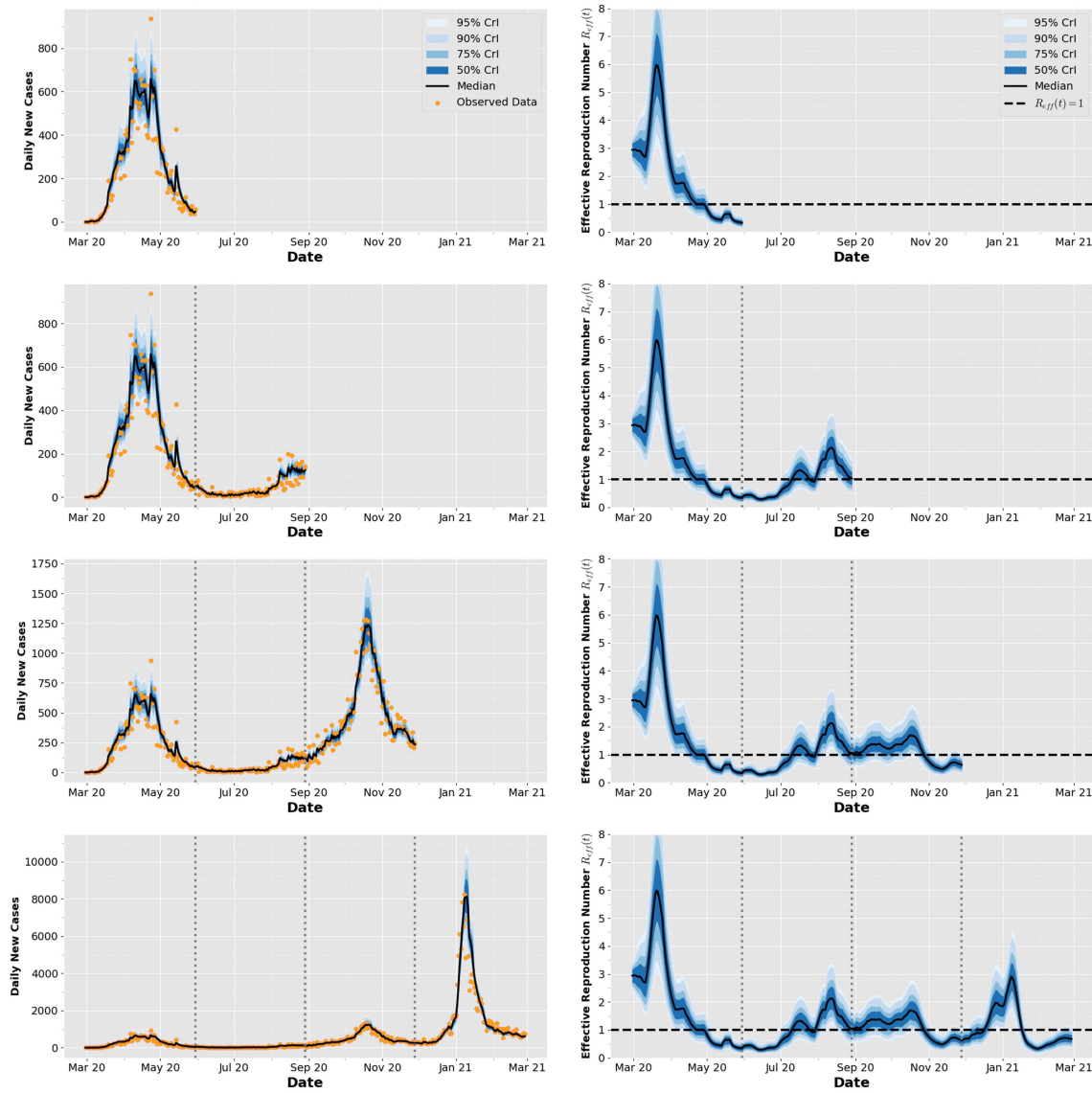


Fig. 1: Real-time application of O-SMC² to sequential data: (Row 1) February 29, 2020, to May 30, 2020; (Row 2) May 30, 2020, to August 29, 2020; (Row 3) August 29, 2020, to November 28, 2020; and (Row 4) November 28, 2020, to February 27, 2021. Each row depicts the sequential estimates of daily new cases and the weekly average effective reproduction number ($R_{\text{eff}}(t)$). The solid black lines represent the median estimate, while the shaded blue regions indicate posterior uncertainty quantiles.

References

Aloke, S.N., Nwaeze, E., Omenyi, L., Uchenna, M., 2023. Parameters estimation of covid-19 seir model. *Asian Journal of Pure and Applied Mathematics* , 229–241.

Althaus, C.L., 2014. Estimating the reproduction number of Ebola virus (EBOV) during the 2014 outbreak in West Africa. *PLoS currents* 6, ecurrents-outbreaks.

Andrieu, C., Doucet, A., Holenstein, R., 2010. Particle Markov Chain Monte Carlo Methods (with discussion). *Journal of the Royal Statistical Society: Series B (Statistical Methodology)* 72, 1–269.

Birrell, P.J., Pebody, R.G., Charlett, A., Zhang, X.S., Angelis, D.D., 2017. Real-time modelling of a pandemic influenza outbreak. *Health Technology Assessment* 21, 1–118. doi:[10.3310/hta21580](https://doi.org/10.3310/hta21580).

Birrell, P.J., Wernisch, L., Tom, B.D., Held, L., Roberts, G.O., Pebody, R.G., De Angelis, D., 2020. Efficient real-time monitoring of an emerging influenza pandemic: How feasible? *The annals of applied statistics* 14, 74.

Calvetti, D., Hoover, A., Rose, J., Somersalo, E., 2021. Bayesian particle filter algorithm for learning epidemic dynamics. *Inverse Problems* 37, Article 115008. doi:[10.1088/1361-6420/ac2cdc](https://doi.org/10.1088/1361-6420/ac2cdc).

Camacho, A., Kucharski, A., A Ki-Sawyerr, Y., White, M.A., Flasche, S., Baguelin, M., Pollington, T., Carney, J.R., Glover, R., et al., 2015. Temporal changes in Ebola transmission in Sierra Leone and implications for control requirements: A real-time modelling study. *PLoS Curr* 7.

Carpenter, B., Gelman, A., Hoffman, M.D., Lee, D., Goodrich, B., Betancourt, M., Brubaker, M., Guo, J., Li, P., Riddell, A., 2017. Stan: A probabilistic programming language. *Journal of statistical software* 76, 1–32.

Cazelles, B., Nguyen-Van-Yen, B., Champagne, C., et al., 2021. Dynamics of the COVID-19 epidemic in Ireland under mitigation. *BMC Infectious Diseases* 21, 735. URL: <https://doi.org/10.1186/s12879-021-06433-9>, doi:[10.1186/s12879-021-06433-9](https://doi.org/10.1186/s12879-021-06433-9).

Chopin, N., 2002. A sequential particle filter method for static models. *Biometrika* 89, 539–552.

Chopin, N., Jacob, P.E., Papaspiliopoulos, O., 2013. SMC²: An Efficient Algorithm for Sequential Analysis of State Space Models. *Journal of the Royal Statistical Society: Series B (Statistical Methodology)* 75, 397–426.

Chowell, G., Bleichrodt, A., Luo, R., 2024. Parameter estimation and forecasting with quantified uncertainty for ordinary differential equation models using quantdiffforecast: A matlab toolbox and tutorial. *Statistics in Medicine* 43, 1826–1848.

Dong, R., Goodbrake, C., Harrington, H.A., Pogudin, G., 2023. Differential elimination for dynamical models via projections with applications to structural identifiability. *SIAM Journal on Applied Algebra and Geometry* 7, 194–235.

Doucet, A., de Freitas, N., Gordon, N., 2001. An Introduction to Sequential Monte Carlo Methods. Springer New York, New York, NY. doi:[10.1007/978-1-4757-3437-9_1](https://doi.org/10.1007/978-1-4757-3437-9_1).

Doucet, A., Johansen, A.M., et al., 2009. A tutorial on particle filtering and smoothing: Fifteen years later. *Handbook of nonlinear filtering* 12, 3.

Dureau, J., Kalogeropoulos, K., Baguelin, M., 2013. Capturing the time-varying drivers of an epidemic using stochastic dynamical systems. *Biostatistics* 14, 541–555. doi:[10.1093/biostatistics/kxs052](https://doi.org/10.1093/biostatistics/kxs052), pmid:[23292757](https://pubmed.ncbi.nlm.nih.gov/23292757/). epub 2013 Jan 4.

Endo, A., van Leeuwen, E., Baguelin, M., 2019. Introduction to particle Markov-chain Monte Carlo for disease dynamics modellers. *Epidemics* 29, 100363.

Funk, S., Camacho, A., Kucharski, A.J., Eggo, R.M., Edmunds, W.J., 2018. Real-time forecasting of infectious disease dynamics with a stochastic semi-mechanistic model. *Epidemics* 22, 56–61. doi:[10.1016/j.epidem.2016.11.003](https://doi.org/10.1016/j.epidem.2016.11.003).

Golightly, A., Kypraios, T., 2018. Efficient smc 2 schemes for stochastic kinetic models. *Statistics and Computing* 28, 1215–1230.

Gordon, N., Salmond, D., Smith, A., 1993. Novel Approach to Nonlinear/Non-Gaussian Bayesian State Estimation. *IEEE Proceedings F – Radar and Signal Processing* 140, 107–113. doi:[10.1049/ip-f-2.1993.0015](https://doi.org/10.1049/ip-f-2.1993.0015).

Grinsztajn, L., Semenova, E., Margossian, C.C., Riou, J., 2021. Bayesian workflow for disease transmission modeling in stan. *Statistics in medicine* 40, 6209–6234.

Han, D., Kim, M., Koh, E., Kobayashi, G., Choi, T., 2025. Sequential monte carlo abc: an overview with application to covid-19 data. *Journal of the Korean Statistical Society* 54, 248–283.

Inouzhe, H., Rodríguez-Álvarez, M.X., Nagar, L., Akhmatkaya, E., 2023. Dynamic SIR/SEIR-like models comprising a time-dependent transmission rate: Hamiltonian Monte Carlo approach with applications to COVID-19. URL: <https://arxiv.org/abs/2301.06385>, arXiv:2301.06385.

Irish Department of Health, 2020. A Population-Level SEIR Model for COVID-19 Scenarios. Available from: www.hse.ie.

Jacob, P.E., 2015. Sequential Bayesian inference for implicit hidden Markov models and current limitations. *ESAIM: Proceedings and Surveys* 51, 24–48.

Jaouimaa, F.Z., Dempsey, D., Van Osch, S., Kinsella, S., Burke, K., Wyse, J., Sweeney, J., 2021. An age-structured SEIR model for COVID-19 incidence in Dublin, Ireland with framework for evaluating health intervention cost. *PLoS One* 16, e0260632. doi:[10.1371/journal.pone.0260632](https://doi.org/10.1371/journal.pone.0260632).

Jewell, C.P., Kypraios, T., Neal, P., Roberts, G.O., 2009. Bayesian analysis for emerging infectious diseases. *Bayesian Analysis* 4, 465–496. doi:[10.1214/09-BA417](https://doi.org/10.1214/09-BA417).

Kantas, N., Doucet, A., Singh, S.S., Maciejowski, J., Chopin, N., et al., 2015. On particle methods for parameter estimation in state-space models. *Statistical science* 30, 328–351.

Karami, H., Bleichrodt, A., Luo, R., Chowell, G., 2024. Bayesianfitforecast: A user-friendly r toolbox for parameter estimation and forecasting with ordinary differential equations. arXiv preprint arXiv:2411.05371 .

Kypraios, T., Neal, P., Prangle, D., 2017. A tutorial introduction to Bayesian inference for stochastic epidemic models using Approximate Bayesian Computation. *Mathematical Biosciences* 287, 42–53.

Lekone, P.E., Finkenstädt, B.F., 2006. Statistical inference in a stochastic epidemic SEIR model with control intervention: Ebola as a case study. *Biometrics* 62, 1170–1177.

Liyanage, Y.R., Saucedo, O., Tuncer, N., Chowell, G., 2025. A tutorial on structural identifiability of epidemic models using structuralidentifiability. jl. arXiv preprint arXiv:2505.10517 .

Marani, M., Katul, G.G., Pan, W.K., Parolari, A.J., 2021. Intensity and frequency of extreme novel epidemics. *Proceedings National Academy Sciences* 118. doi:[10.1073/pnas.2105482118](https://doi.org/10.1073/pnas.2105482118).

Minter, A., Retkute, R., 2019. Approximate bayesian computation for infectious disease modelling. *Epidemics* 29, 100368.

O'Neill, P.D., Roberts, G.O., 1999. Bayesian inference for partially observed stochastic epidemics. *Journal of the Royal Statistical Society Series A: Statistics in Society* 162, 121–129.

Pitt, M.K., Shephard, N., 1999. Filtering via Simulation: Auxiliary Particle Filters. *Journal of the American Statistical Association* 94, 590–599. doi:[10.1080/01621459.1999.10474153](https://doi.org/10.1080/01621459.1999.10474153).

Roberts, M., Andreasen, V., Lloyd, A., Pellis, L., 2015. Nine challenges for deterministic epidemic models. *Epidemics* 10, 49–53.

Rosato, C., Varsi, A., Murphy, J., Maskell, S., 2023. An $o(\log 2 n)$ smc 2 algorithm on distributed memory with an approx. optimal l-kernel, in: 2023 IEEE Symposium Sensor Data Fusion and International Conference on Multisensor Fusion and Integration (SDF-MFI), IEEE. pp. 1–8.

Sauer, T., Berry, T., Ebeigbe, D., Norton, M.M., Whalen, A.J., Schiff, S.J., 2021. Identifiability of infection model parameters early in an epidemic. *SIAM journal on control and optimization* 60, S27–S48.

Sheinson, D.M., Niemi, J., Meiring, W., 2014. Comparison of the performance of particle filter algorithms applied to tracking of a disease epidemic. *Mathematical Biosciences* 255, 21–32. doi:<https://doi.org/10.1016/j.mbs.2014.06.018>.

Storvik, G., Diz-Lois Palomares, A., Engebretsen, S., Rø, G.Ø.I., Engø-Monsen, K., Kristoffersen, A.B., De Blasio, B.F., Frigessi, A., 2023. A sequential Monte Carlo approach to estimate a time-varying reproduction number in infectious disease models: the Covid-19 case. *Journal of the Royal Statistical Society Series A: Statistics in Society* 186, 616–632.

Toni, T., Welch, D., Strelkowa, N., Ipsen, A., Stumpf, M.P., 2009. Approximate bayesian computation scheme for parameter inference and model selection in dynamical systems. *Journal of the Royal Society Interface* 6, 187–202.

Vieira, R.M., 2018. Bayesian online state and parameter estimation for streaming data. Ph.D. thesis. Newcastle University.

Wang, S., Walker, S.G., 2022. Bayesian Data Augmentation for Partially Observed Stochastic Compartmental Models. URL: <https://arxiv.org/abs/2206.09018>, [arXiv:2206.09018](https://arxiv.org/abs/2206.09018).

Welding, J., Neal, P., 2019. Real-time analysis of epidemic data. arXiv preprint arXiv:1909.11560 doi:[10.48550/arXiv.1909.11560](https://arxiv.org/abs/1909.11560).

World Health Organisation (WHO), 2024. Coronavirus Disease (COVID-19) Pandemic. <https://www.who.int/emergencies/diseases/novel-coronavirus-2019>. Last accessed on 2024-03-1.

Yang, W., Karspeck, A., Shaman, J., 2014. Comparison of Filtering Methods for the Modeling and Retrospective Forecasting of Influenza Epidemics. *PLoS Comput Biol* 10, e1003583. doi:[10.1371/journal.pcbi.1003583](https://doi.org/10.1371/journal.pcbi.1003583).